

Pipeline Flaw Detection Using Shear EMAT and Wavelet Analysis

Venugopal K. Varma^{*}, Raymond Tucker¹, Steve Kercel², Joseph Rose³, Wei Luo³, and Xiaoliang Zhao⁴

ABSTRACT

This paper describes the development of an EMAT based PIG for in-line inspection of flaws in a 30 inch natural gas pipeline. The sensor is capable of detecting physical flaws (e.g., SCC, circumferential and axial flaws, and corrosion) in pipe walls of gas pipelines. Using an in-line non-contact ultrasonic sensor (EMAT) flaws are determined in the wall of the pipe that the current MFL technology has problems detecting. One EMAT is used as a transmitter, exciting an ultrasonic impulse into the pipe wall while a second EMAT located a few inches away from the first, is used as a receiving transducer. This paper reports on the identification of flaw signatures in the receiver output. Since the discrete wavelet transform of the signal will be non-shift invariant, its coefficients cannot be directly used as a pattern recognition feature. However, comparing composite properties of the signal on different scales is useful, because the mode conversion caused by a flaw changes the composite properties of the signal in wavelet space. For the EMAT data, the useful information projects onto five mutually orthogonal wavelet scales. This paper also presents the results of 3D modeling using BEM performed on a horizontal guided wave incident on a flaw.

* Corresponding author (varmavk@ornl.gov)

¹ Oak Ridge National Laboratory, Oak Ridge, TN 37831

² Endogenous Systems Research Group, University of New England

³ Pennsylvania State University, University Park, PA

⁴ Intelligent Automation, Inc., Rockville, MD

1.0 INTRODUCTION

The safety of the United States' natural gas supply is of prime importance, since 30 percent of the energy produced in the country is derived from it. Natural gas is supplied through a million miles of vast pipeline network [1]. Pipeline companies have an impressive safety record due to the proactive role of standards and pipeline inspection. Since our pipelines are getting old, there is a great need to identify corrosion, cracks, and other defects that pose potential problems.

Stress corrosion cracks (SCC) can occur in a range of pipeline field conditions including soil type, stress, cathode potential, coating conditions and temperature. This type of defect is usually oriented along the axial length of the pipe. If the defect remains undetected the cracks may grow and/or coalesce and eventually lead to a leak or pipe rupture. Other types of defects can also occur in pipe structures. They are either critical to the safety of the pipeline (e.g., corrosion, welding cracks, and pits) or benign stringer-like internal inclusions. Non-destructive Inspection (NDI) systems are vital to locating the defects early without false alarms from benign inclusions to problematic cracks as well as helping characterize and size the defects for repair or replacement.

Many technologies have been developed for pipe inspections, but they are limited to detecting certain types of defects. For example, *Axial-field Magnetic Flux leakage (MFL) in-line inspection smart pipe-inspection-gears (PIG)*, which is extensively used for pipeline inspection, is good for detecting corrosion damage or circumferentially oriented defects inside a pipe, but have limited success in detecting flaws or cracks in the axial direction.

In this project, ultrasonic guided waves are being studied for the feasibility of detecting many kinds of defects that occur in pipes. One major benefit of guided waves is their rapid global inspection capability, which enables them to inspect a structure line-by-line instead of point-by-point. However, defect classification and sizing by guided waves are still major problems under investigation, due to the complexity of the wave propagation characteristics.

2.0 BACKGROUND

There are two main ways of testing the integrity of pipelines. One is destructive inspection and the other is non-destructive testing. The destructive testing procedure uses hydrostatic inspection to verify that a pipeline is within the safety margin for operation. The procedure does not, however, locate defects that are just above the threshold of the safety margin. In addition, destructive testing requires the disruption of a pipeline's normal operation and, for this reason, is not a preferred method. Generally, such techniques are good for offline inspection of pipelines before they are put into use. Non-destructive inspection (NDI) technique detects flaws that can cause failure in the future. This way, NDI provides information on the integrity of the pipeline as well as a measure of its current safety margin.

A pipeline that is in service can fail due to many causes. Some of the most common failure modes are corrosion, pitting, SCC, seam weld cracks, dents, and other flaws due to external impact from earth-moving equipment. Ideally, it is prudent to detect all of the above cracks, but

a technique used for detecting a particular flaw is not ideally suited to detect another. Hence, the natural gas industry uses a combination of techniques to ensure the safety margin for their operation. The probabilistic approaches have also been used for estimating pipeline integrity [2]. Probabilistic method attempts to predict safety using crack rate growth, inspection frequency, and operating parameters of the pipe. Researchers are also working on variations of different approaches exploiting various phenomena of a particular technique, to extract more information on pipeline integrity. The goal of such research is to improve the performance of the sensor without a complete redesign of the system.

The non-destructive testing of pipes can be broadly classified as the MFL method or the ultrasonic guided wave approach. These classifications can be further subdivided as follows:

- Magnetic Flux Leakage
 - Induction Coil Method
 - Hall Effect Method

- Ultrasonic Method
 - Contact → Piezoelectric
 - Lamb Wave
 - Shear Horizontal Wave

 - Non-Contact → EMAT, Magnetostrictive Sensor
 - Longitudinal Guided Wave
 - Shear Horizontal Wave

3.0 WORKING PRINCIPLE OF EMAT

Ultrasonic waves traveling through the walls of the pipe will be affected by the features they encounter and can be measured to interpret the condition of the pipe. The most common way of generating an ultrasonic wave is to use a piezoelectric device.

Piezoelectric devices need contact with the material to provide a good coupling to induce an ultrasonic wave. Generally, a liquid medium (e.g., oil, grease) is used to obtain this contact. In an instrument that is moving along the length of the pipe, getting a good contact has been difficult. Hence, most NDI measurements for pipe inspection have relied on MFL technology. The PII Group, U.K., has circumvented this problem by employing a liquid-filled wheel contacting the walls of the pipe. The piezoelectric wave generator is situated inside the wheel, and the liquid provides a good coupling mechanism for its transmission and reception. This methodology is employed in their elastic wave vehicle design. A newer method of ultrasonic testing that is gaining momentum is the EMAT (electromagnetic acoustic transducer) wave generator. The basic principle of EMAT is that a conductor carrying current near the surface of a metal under a magnetic field will induce an electromagnetic force given by the Lorentz equation [3]. Also, if the material is ferromagnetic, a magnetostrictive effect takes place that can be five

times more powerful than the Lorentz forces. This combination of forces acting on the material will generate Lamb, Shear, and Longitudinal ultrasonic waves in the material, depending on the configuration of the magnet and the direction of the current flow. Since the EMAT transducer does not touch the material being inspected, the main drawback of the piezoelectric ultrasonic is overcome with this approach. The signal an EMAT generates is not as strong as those obtained by other means and hence, extra care must be employed in the signal processing and power conditioning circuits when using this approach (see Figure 1).

The ultrasonic guided wave technique has been used for locating defects in boiler tubes [4, 5], determining bolt axial stress [6], and inspecting pipeline [7, 8, and 9]. Operating frequency, wave-packet size, and the distance to the sensor all affect the dispersion characteristic of ultrasonic waves [10]. Ideally, the dispersion of an acoustic wave needs to be minimized. Another characteristic that is of importance is the wave mode used for testing. Most researchers have used either the Shear n_0 or the n_1 in their experiments since, by operating the EMAT at these frequencies, multiple mode generation could be avoided. Higher operating frequencies will result in multiple modes being generated. There have been many recent developments in the manufacturing of the EMAT ultrasonic generator [9, 10]. Sawaragi [10] talks about using an eight-element probe instead of a four-element probe, and Hamilton [9] discusses using a chirp signal to generate the input signal where an ultrasonic wave sweeps linearly over a range of operating modes (due to change in frequency). Along the lines of the EMAT, Kwun [11, 12] generated a longitudinal wave using magnetostrictive sensors. Apart from longitudinal and shear waves, Lamb waves produced with EMATs have also been used to study material defects and characterization [13, 14, 15].

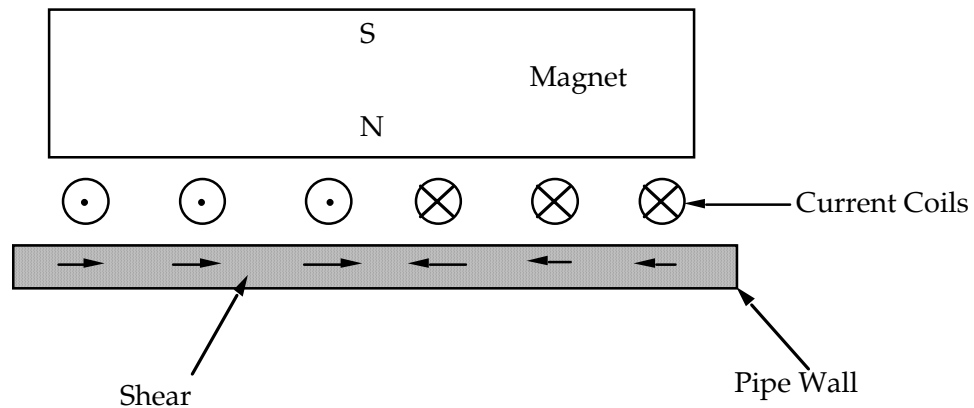


Fig. 1. Schematic of an EMAT Transducer.

3.1 Lorentz Force Type EMAT Design

For non-ferromagnetic materials, EMATs work on the basis of a Lorentz force mechanism, whereas in ferromagnetic materials both Lorentz force and magnetostriction have to be considered. Consider a case where an EMAT works on the basis of Lorentz force and quasi-static conditions.

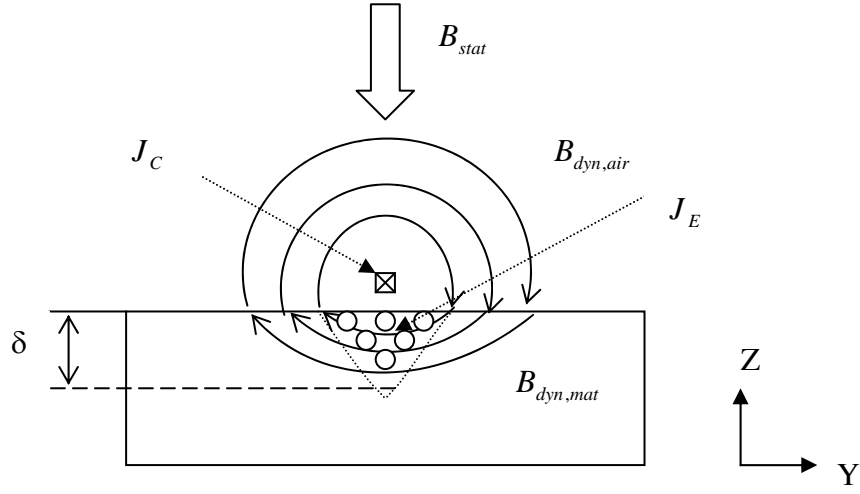


Fig. 2. Elementary setup of an EMAT transducer.

Figure 2 shows a current carrying wire held close to the surface of a conducting material and a source for a static field, such as a permanent magnet or an electromagnet. An alternating current I_T is sent through the wire. The current density $\vec{J}_{C,T}$ in the conductor generates a dynamic magnetic induction $\vec{B}_{dyn,T}$ in the surrounding air and in the conducting material, according to Maxwell's law ^[4]

$$\begin{aligned} \text{rot } \vec{H}_{dyn,T} &= \vec{J}_{C,T}, \\ \vec{B}_{dyn,air,T} &= \mu_{air} \vec{H}_{dyn,T}, \\ \vec{B}_{dyn,mat,T} &= \mu_{mat} \vec{H}_{dyn,T}. \end{aligned}$$

The time-varying magnetic field induces eddy currents in the electrically conductive materials given by

$$\begin{aligned} \text{rot } \vec{E}_{E,T} &= -\frac{\partial \vec{B}_{dyn,T}}{\partial t}, \\ \vec{J}_E &= \gamma \vec{E}_{E,T}, \end{aligned}$$

where γ is the conductivity of the material. The penetration depth of the eddy currents is given by the classical skin-depth

$$\delta = \frac{1}{\sqrt{\pi f \gamma \mu_{mat}}}.$$

The Lorentz force density

$$\vec{f}_L = \vec{J}_{E,T} \times (\vec{B}_{Stat,T} + \vec{B}_{dyn,T})$$

is proportional to the sum of the static magnet field of the permanent magnet or electromagnet and the dynamic magnet field of the conductor, and is exerted on the lattice of the material under the conductor. The Lorentz force density in turn gives rise to an ultrasonic wave being launched in the material. In the case of an EMAT as a receiver of ultrasonic waves, the setup is essentially the same as for the transmitting case. When an ultrasonic wave travels in the

material under the receiving conductor with speed vector \vec{v} , locally, in the magnetic field of the receiver, a time-varying eddy current density

$$\vec{J}_{E,R} = \gamma \vec{v} \times \vec{B}_{stat,R}$$

is induced in the material. The eddy current has an associated magnetic field intensity and induction inside the material and in the surrounding air, given by

$$\begin{aligned} rot \vec{H}_{dyn,R} &= \vec{J}_{C,R}, \\ \vec{B}_{dyn,air,R} &= \mu_{air} \vec{H}_{dyn,R}, \\ \vec{B}_{dyn,mat,R} &= \mu_{mat} \vec{H}_{dyn,R}. \end{aligned}$$

The time-varying magnetic induction in the air induces an electric field in the receiving conductor, which gives rise to a current density

$$\begin{aligned} rot \vec{E}_{E,R} &= -\frac{\partial \vec{B}_{dyn,R}}{\partial t}, \\ \vec{J}_{C,R} &= \gamma \vec{E}_{C,R}. \end{aligned}$$

4.0 MODELING OF ULTRASONIC SHEAR WAVES

A two-dimensional hybrid Boundary Element Method (BEM) combined with the normal mode expansion technique has been used to study the Lamb wave mode conversion from the edge of a plate [16] and the interaction with surface-breaking defects [17]. The initial work on shear (SH) wave sizing potential was also reported in Rose and Zhao [18], where the same technique was used to study the interaction of the n_0 mode SH wave with various crack and corrosion boundaries in a structure. All these studies showed great potential of guided waves for solving the defect characterization and sizing problem.

In reality, all defects are in three dimensions. Although we can approximate the defects with widths much larger than the beam width as 2D defects, there are defects that are either narrower than the beam width or non-uniform in the width direction. So a 3D model is needed to characterize these defects. The three-dimensional guided wave propagation characteristics were not studied well until recently, due to the greater need for defect characterization. Achenbach [19] decomposed the Lamb wave displacement as a thickness motion and a membrane carrier wave that defines the propagation along the plate. Using this method, Achenbach and Xu [20] studied the wave motion in an isotropic elastic layer generated by a time-harmonic point source load of an arbitrary direction. Earlier, Chang and Mal [21] also developed the 3D global functions for Lamb waves in order to calculate the wave scatterings from a rivet hole without an edge crack on a plate by the finite element method. Their measured histories and spectra of the transmitted and reflected waves agreed well with the calculation from their hybrid model. Fromme and Sayir [22] published their experimental measurement of scattered Lamb waves by a through hole in a plate; and Diligent et al [23] presented their research on this topic and pointed out the existence of mode converted SH modes from S_0 mode Lamb wave incidence.

Notice that the defects in all of these studies are actually 2D in the sense that they are through holes in a plate having uniform thickness. The present work focuses on a true 3D hybrid BEM code development and applications to 3D defect characterization in a plate. Guided plane waves

are assumed impinging onto a defect. An imagined circular disc region will enclose the defect. The surface of the region, as well as the defect will be meshed using quadrilateral elements and calculated by BEM. Outside the region, both incident and scattered waves will be expanded as superposition of all possible propagating Lamb and SH waves. The constitutive relation between each mode stress and displacements will serve as compatibility boundary conditions at the imaginary boundary. Thus, the amplitude of each mode can be calculated and used as features for classification and sizing.

4.1 Two Dimensional Model

BEM analysis is used to model the flaws and study the effects of guided shear waves impinging on the flaw. The dispersion curves of the circumferential guided SH waves were calculated to arrive at the EMAT settings for generating n_1 mode. Comparison of the dispersion curves with those of a flat plate shows that a large diameter thin-walled pipe can be approximated as a plate locally (see Figure 3). The transmission and reflection coefficient for the SH wave incident on a crack 1/8 inch wide are as shown in Figure 4. These were calculated using 2D BEM analysis. As can be seen from Figure 4, measurement of the transmitted signal can be used to quantify the crack depth.

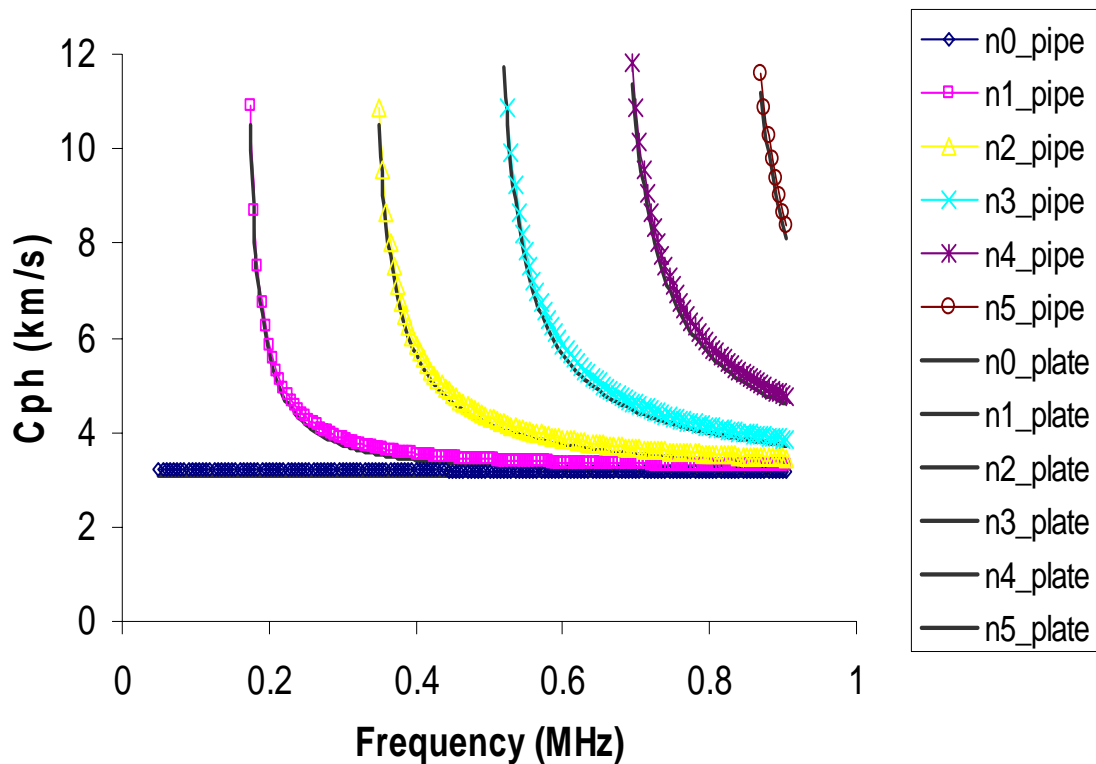


Fig. 3. Phase velocity dispersion curves for SH wave in the circumferential direction of a 10 inch schedule 40 steel pipe and plate of same thickness (9.271mm).

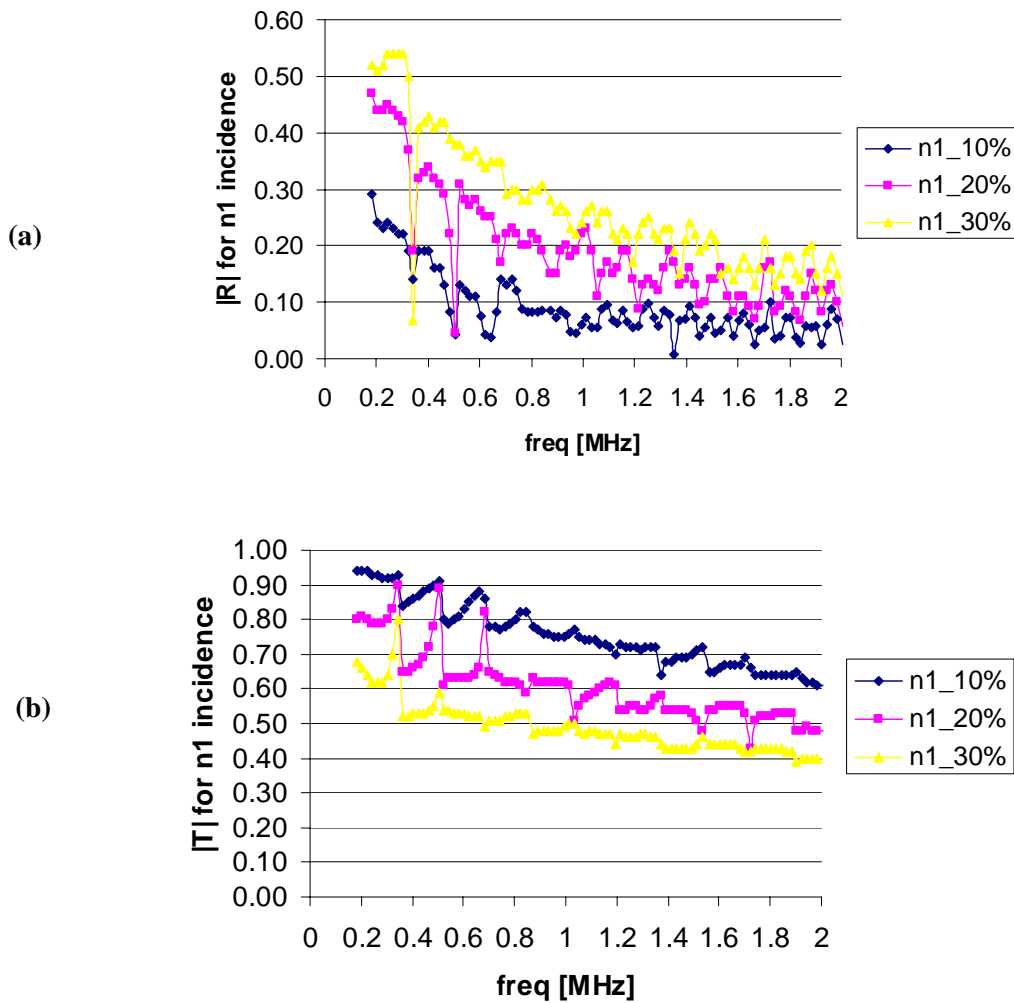


Fig. 4. (a) The reflection coefficient and (b) transmission coefficient of n_1 mode for n_1 mode SH wave incident into 1/8 inch wide cracks with 10%, 20% and 30% through wall depth. The pipe wall is 0.365 inches (9.272 mm) thick.

4.2 Three Dimensional Modeling of Flaws

The geometry for the 3D problem is shown in Figure 5. A cylindrical coordinate system is attached to the center of the meshed disc region, with the $z=0$ plane being the mid-plane of the plate. A commercial Finite Element Analysis package called IDEAS was used to mesh the surface of the disc with defects. Quadrilateral 2D elements were used. The software package can output the coordinates of each corner point and the connectivity relation between elements and corner points was also given. This information can be input to the 3D BEM code as geometry mesh. Consider a time-harmonic SH plane wave incident from the left incident on the hole, the scattered wave field may consists of Lamb waves and SH waves.

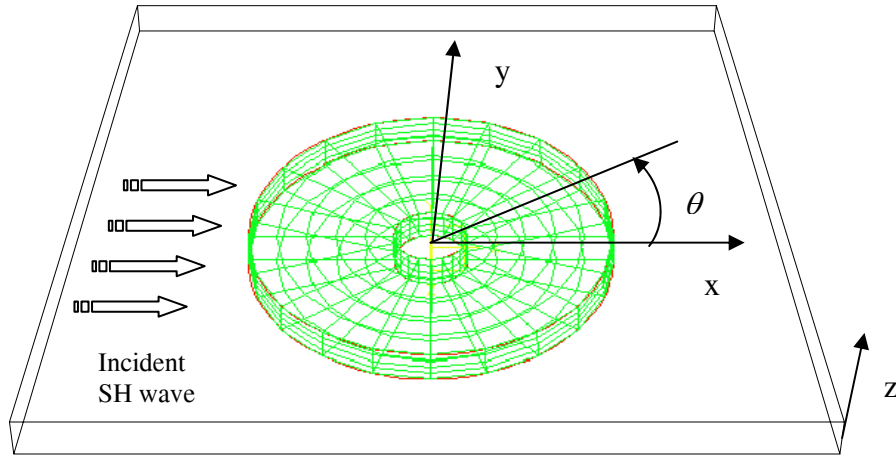


Fig. 5. An example mesh for a 3D defect in an infinite plate. A plane SH wave is incident on the defect region.

As a first step, a 3D elasto-dynamic boundary element code was developed based on the Dominguez's CONDTHEH code. To ensure its validity, a simple numerical experiment was performed using the disk-with-a-hole mesh as shown in Figure 5, which consists of four elements in the thickness direction, twenty elements in the circumferential direction, and six elements in the radial direction. In all, there are 360 boundary elements in the mesh. Boundary conditions are defined as traction free on the top, bottom of the disk and the cylindrical hole. A unit displacement in the x directional is assumed on the virtual cylindrical boundary. The disk material was assumed to be made of mild steel with a longitudinal and shear velocity of $5.9 \text{ mm} / \mu\text{s}$ and $3.2 \text{ mm} / \mu\text{s}$ respectively. A wave frequency (f) of 0.5 MHz was assumed for this analysis.

It is seen that all three traction components are roughly symmetric with respect to the x axis, which should be obvious because of the symmetric displacement boundary condition. In addition, the x and z traction components are maximized at 0° and 180° while the y traction component is maximized at 45° , 135° , 225° , and 315° . This is also reasonable because the x traction component will be a reflected maximum at 0° and 180° degrees from the inner hole and converts to a maximum to the y component traction at 45° , 135° , 225° , and 315° . The relative amplitude of the traction components also indicates that the calculation is credible.

The hybrid boundary element normal mode expansion technique was applied to the calculation of the scattered wave field from a circular through-plate hole in a plate. The scattered wave has two major components: one is the S_0 mode Lamb wave and the other is the n_0 mode SH wave. It is clear that mode conversion occurs at the defect boundary from the S_0 mode Lamb wave to n_0 mode SH wave, since the incident wave consists only the S_0 mode Lamb wave. This phenomenon does not happen in the 2D model because the vibration in the wave propagation direction could not be converted to the vibration that is

perpendicular to it. In addition, since the defect is a through-plate hole that is uniform in the plate thickness direction, no mode conversion occurs from S_0 mode to A_0 mode, and all amplitudes of the angular components are close to zero. This is only true for defects whose shape is invariant in the thickness direction and through the plate. One should not extend it to arbitrary shaped defects that do not have that property.

5.0 EMAT SENSOR DEVELOPMENT

EMAT sensors were designed for 10 inch and 12 inch pipe geometry with hardware fabricated for attaching them onto the inside walls of the pipe. The anchoring mechanism had provisions to vary the gap between the pipe wall and the EMAT. With wheels or ball rollers, the EMATs could be positioned anywhere inside the pipe. Figure 6 shows the circumferential and axial EMATs developed for pipeline inspection. A separation of 6 inches between the transmitter and receiver was used for both configurations.

Cuts of 0.125, 0.25, and 0.006 inch wide and varying depths were fabricated on the pipe walls to determine whether the EMATs were able to detect these flaws. Most tests were performed using horizontal n_1 mode SH wave. By utilizing the through-transmission mode whereby the distance between the EMATs is fixed, better correlation was obtained for the effect of flaws. A sample of the windowed receiver pulse signal for the cases of *flaws* and *no-flaws* on the pipe walls is given in Figure 7. As can be seen from the Figure 10, the signal is strongest when there is no flaw and reduces in amplitude when it encounters a flaw.

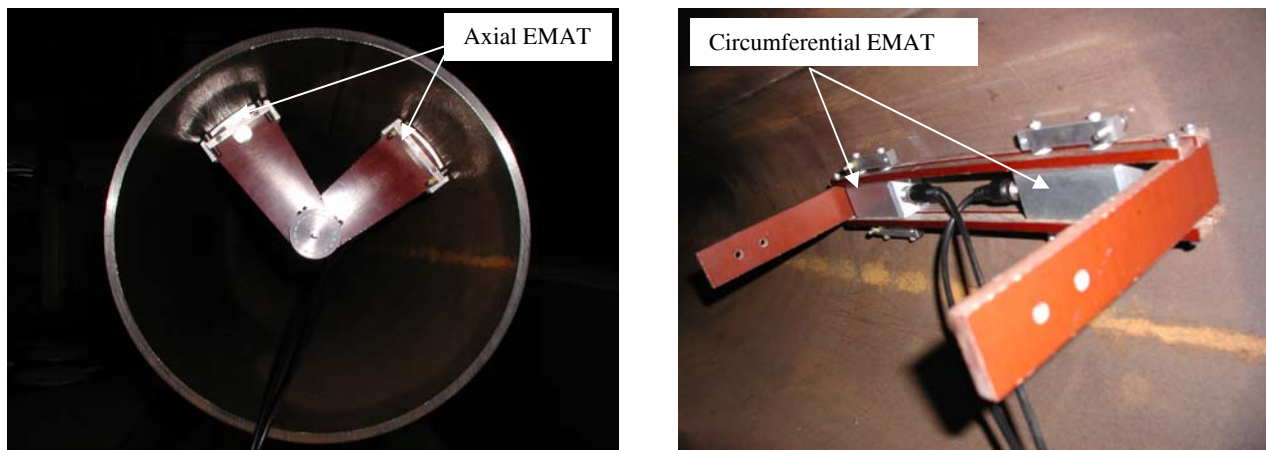


Fig. 6. Axial and Circumferential EMATs.

The multiple pulses in SCC flaw data are due to the smaller section of the pipe used for this case — 18 inches instead of 6 feet. These pulses correspond to the reflections from the pipe ends and are separated by larger time intervals when the pipe section used is long. The number of EMATs required to characterize the entire diameter of the pipe was determined by assessing the propagation angle that does not adversely affect the quality of the signal for preset EMAT separation. For axial EMAT configuration, the axial separation could be 2 inches without large degradation of the receiver signal while, in case of the circumferential EMAT, the angular separation could be $\pm 30^\circ$.

Attenuation or changes in amplitude in the time domain data (see Figure 7) are not a useful feature for identifying flaws. Despite the fact that such changes are obvious in laboratory data, which are collected under carefully controlled conditions, their reliability does not hold up for data collected in less controlled field conditions. Too many other mechanisms besides a flaw in the medium of propagation can lead to attenuation in field data. The only reliable features for flaw detection are those that depend on the change imposed by the flaw on the shape rather than the amplitude of the signature.

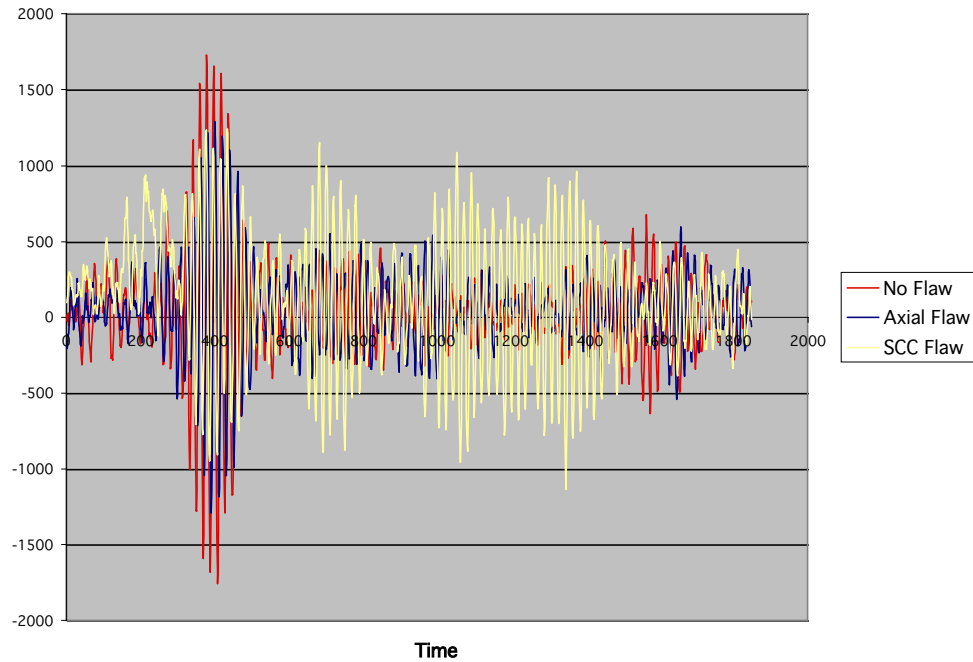


Fig. 7. Amplitude versus time for *flaw* and *no-flaw* receiver EMAT signal.

After the initial development of the EMAT sensors for the 10 inch and 12 inch pipes, sensors were developed to inspect a 30 inch pipe with the PIG traveling along the length of the pipe (see Figures 8 & 9). An industrial computer, EMATs, resolver, and control box were all mounted on a frame that could travel along the inside of a 30 inch pipeline and characterize the wall defects. The schematic of the experimental PIG developed at ORNL is shown in Figure 8. The EMATs are mounted on linear springs that ensure that the distance between the pipe inside wall and the EMAT surface is maintained as tightly as possible. The receiver and the transmitter radial positions are controlled independently to account for the geometric variation of the pipe diameter. The separation distance between the transmitter and the receiver can be adjusted and, the current setting of 10 inch circumferential separation ensures that the excitation signal does not overlap with the transmitted chirp signal.

A windowed SH wave generated every 12 milliseconds is sampled at 5 MHz frequency by the data acquisition system. When the PIG is traveling at 2 miles per hour a sample is taken every 0.42 inches of travel. A LabView program is used to gather the data from the data acquisition board and write it to a disk file. The data collected will be evaluated offline to detect flaws in the pipeline using wavelet analysis.

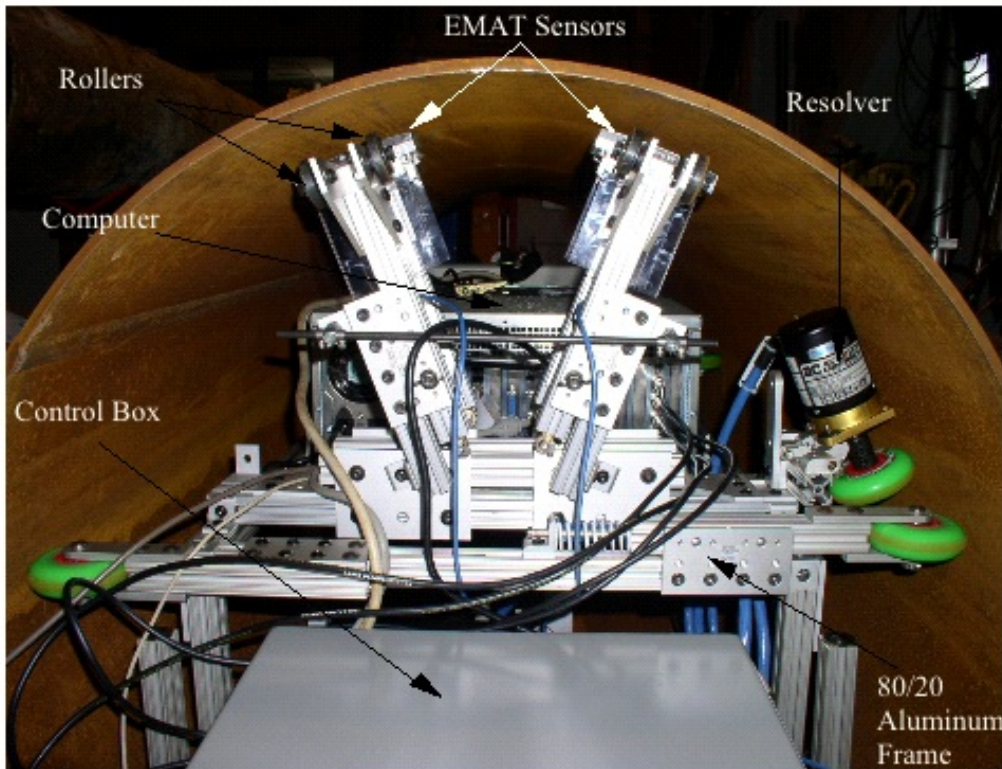


Fig. 8. ORNL PIG with EMAT sensors and resolver mounted inside a 30 inch pipe.

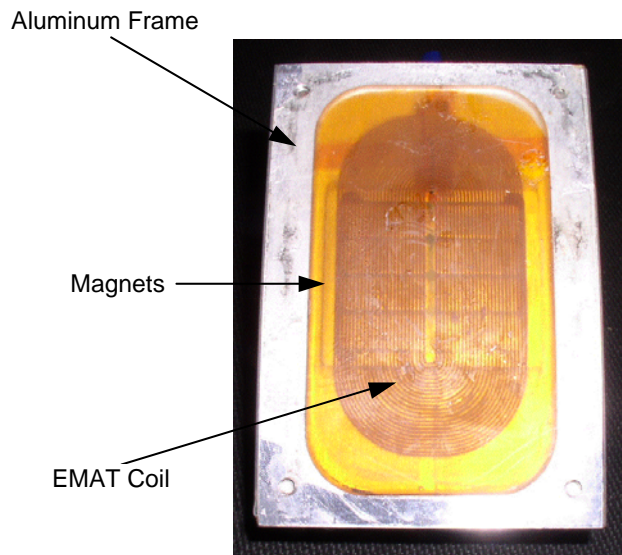


Fig. 9. EMAT used for the 30 inch pipe defect characterization.

The current set-up is used to evaluate the defects that exist in the 10 inch circumferential distance between the transmitter and the receiver EMATs. The receiver EMAT on the 30 inch pipe wall will also obtain the signal that is traveling the 84.25 inch circumferential path, but the signal would be too weak to be used for flaw classification. Hence, for a field-deployable flaw classification and characterization PIG, multiple pairs of EMATs will be installed.

6.0 WAVELET ANALYSIS

To find features that distinguish the presence of a flaw, the signal must be analyzed and literally broken apart. The most useful technique for performing such an analysis is the discrete wavelet transform [24]. In mathematics, the wavelet function $\psi(t)$ is any complex-valued function ψ of a complex variable that meets two conditions. The function has zero average value; hence it must oscillate. It must have finite energy; hence, it must be a windowed burst. Infinitely many functions meet that condition, but only a fraction of that infinitude is useful for engineering applications.

After determining the wavelet function that is suitable for the signal of interest, the number of wavelet scales required to fully represent the signal is decided. Wavelet features that were used in the classification of the flaws were energy, entropy, phase, and frequency. The idea in pattern recognition is that the *no-flaw* signals will be similar to each other. They will concentrate in a bounded region of feature space relatively close to a cluster center. In the case of an N-dimensional feature space, if the feature dimensions were on the same scale, the feature vectors for the *no-flaw* signals would form a cluster inside some N-dimensional hypersphere whose center is the “cluster center,” and is located at the *mean* of the feature vector values of all the *no-flaw* samples. *Flaw* signals will have feature vectors that are scattered all over the feature space and at some distance from the *no-flaw* cluster center, outside the hyperspherical *decision surface*.

It is worth mentioning that these can lead to multi-dimensional clusters with grossly different scales in the different dimensions. Thus, instead of a hypersphere, the decision surface is an N-dimensional hyperellipse. Matters are further complicated by the fact that the major and minor axes of the ellipse may not align with the coordinate axes of the feature space. The two-dimensional version of the situation is shown in Figure 10.

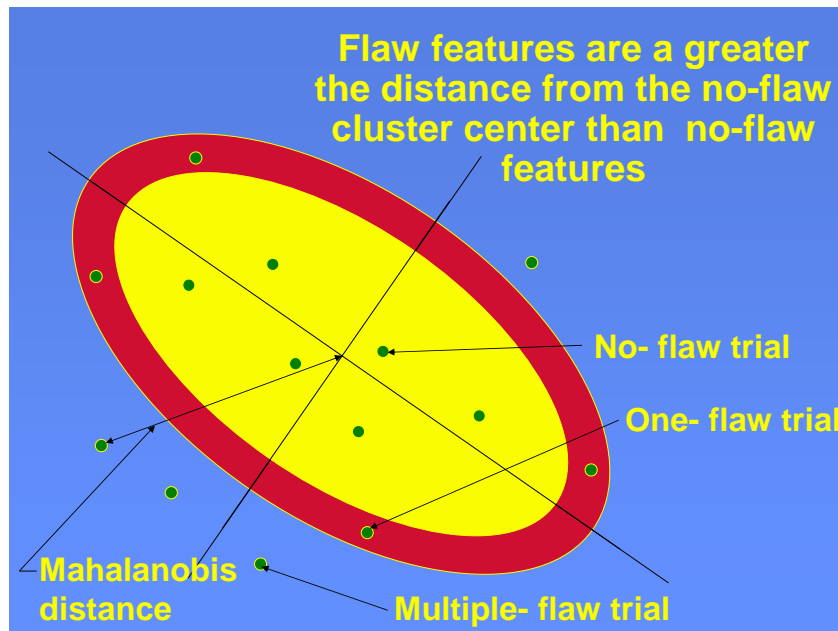


Fig. 10. Clustering of features.

The feature space can be transformed by rotating its coordinate axes to align with the eigenvectors of the covariance matrix of the *no-flaw* features and by rescaling all axes to the same scale. As a result, the distance of any feature vector from the cluster center can then be represented as a single number, conventionally known as the Mahalanobis distance.

6.1 Wavelet Analysis of Experimental Data

The above wavelet analysis was performed on the data obtained using shear EMATs on 10 inch and 12 inch diameter pipes with fabricated flaws. As shown in Figure 11, all the experimental data collected so far can be readily classified. In each plot, the horizontal axis is the fraction of signal energy retained in wavelet-packet space for the analysis. The vertical axis is the squared Mahalanobis distance of the feature vector from the cluster center of the *no-flaw* samples. There is one line on the graph for each trial. The line represents the Mahalanobis distance of the feature vector from the *no-flaw* cluster center, as a function of retained energy.

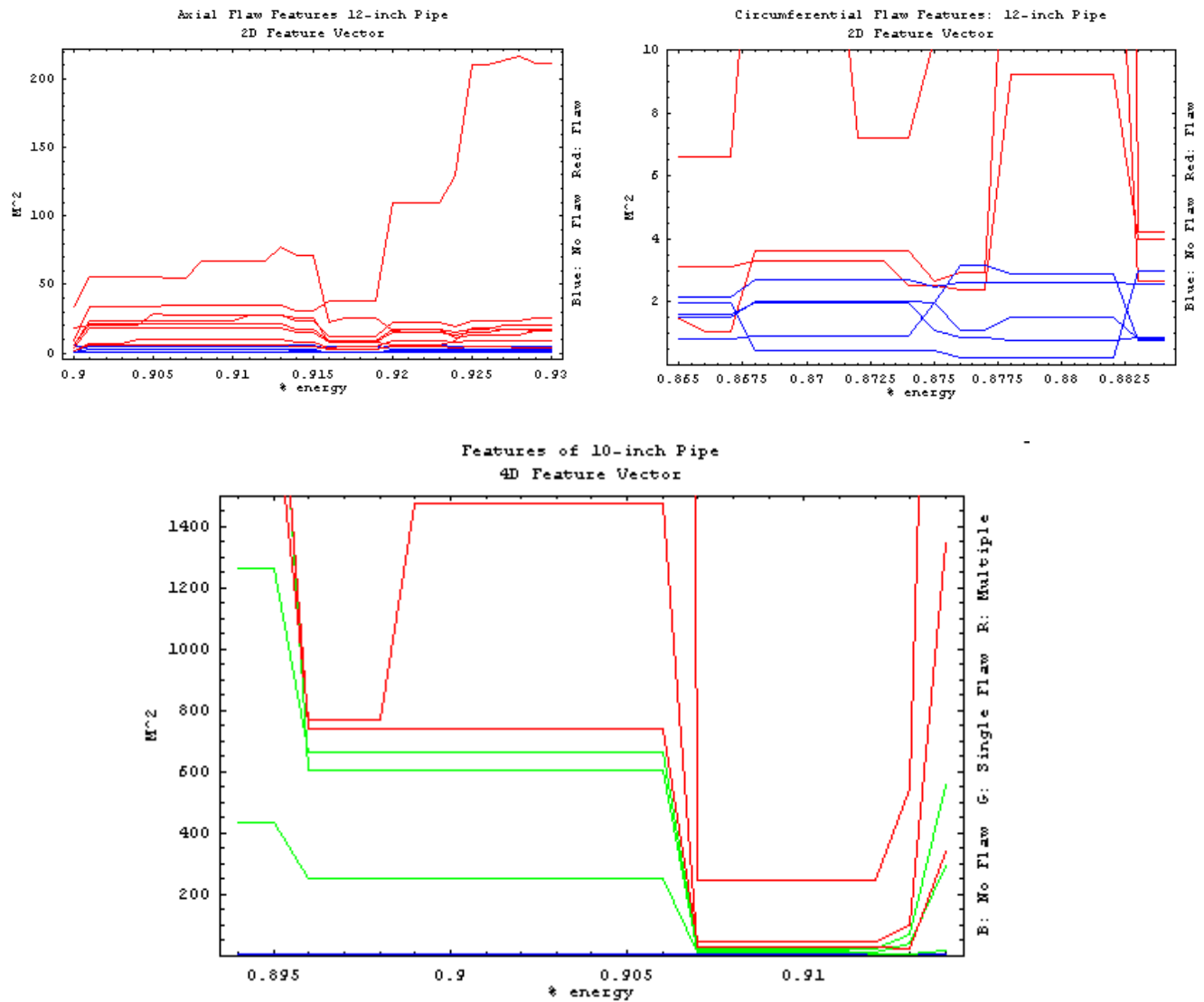


Fig. 11. Mahalanobis distance for Axial, Circumferential and SCC crack Flaws.

Signatures for axial flaw data for the 12-inch pipe were fully distinguished by the following procedure. A 20-coefficient Daubechies wavelet filter was used for processing the data. For the input signal, the analysis uses samples 280 to 919 of the original signal. It takes a best-basis wavelet-packet transform of the 640-sample signal, and keeps the largest coefficients that contain a fraction of the original signal energy in the neighborhood of 90% (zeroing out all the smaller wavelet packet coefficients). The entropies of those larger coefficients for wavelet packet scales 2, 3, and 4 were computed, yielding a 3D feature vector for each trial. The two classes (*flaw* and *no flaw*) are separable in the 3D feature space. The entropies of the larger coefficients for wavelet-packet scales 2 and 3 were also computed, yielding a 2D feature vector for each trial. The two classes (flawed and unflawed) are separable in the 2D feature space, but over a narrower range of retained energies than for the 3D feature vector. Signatures for circumferential flaw data for the 12-inch pipe were fully distinguished by an analysis similar to that described above. A 78-coefficient Coiflet filter was used for processing this data. The 2D feature vector was computed from entropies of wavelet-packet scales 2 and 3.

Signatures for the 10-inch pipe were fully distinguished into three classes (*no flaw*, *single flaw*, and *multiple flaws*) by an analysis similar to that described above. An 8-coefficient Least Asymmetric wavelet filter was used for the above case. For the input signal, the analysis used samples 441 to 760 of the original signal. The entropies of those larger coefficients for wavelet packet scales 2, 3, 4, and 5 were computed yielding a 4D feature vector for each trial.

Signal processing is faced with two distinct problems. One is to distinguish *flaw* versus *no-flaw* signatures. The other is to distinguish "flaw" signatures by flaw type, perhaps 4-6 different classes of flaws. The *flaw* versus *no-flaw* classification must be done in real-time by a microprocessor aboard the PIG. This is constrained by the fact that when the PIG is running down the pipe, it is collecting hundreds of signatures per second, and each signature is a vector of several hundred to several thousand floating point numbers. The PIG runs through the pipe at 2 to 10 feet per second for tens to hundreds of miles without human intervention, and it would be unfeasible to store all the signature data collected during the run for post-processing. Thus, at minimum, the on-board processor must identify the *flaw* signatures in real-time and store them while discarding the *no-flaw* signatures.

For each flaw type and pipe size, a feature space was found in which to distinguish *flaw* from *no-flaw* signatures. Recently, a single feature space was determined in which *flaws* can be readily distinguished from *no-flaw* signatures.

Ideally, the classification by flaw type will also be done on board the PIG. If so, all that gets reported at the end of the run is a list of flaw types and place-of-occurrence. If this proves to be unreliable in practice, then the flaw signatures will be recorded and classified by a slower algorithm after the run.

7.0 CONCLUSION

An EMAT sensor to classify flaws in pipelines has been successfully developed. Corrosion, SCC, and gauges were the flaw types used for this study. Modeling of the guided SH wave propagation in steel plates was used to obtain the dispersion curve and identify the fundamental modal frequencies. 2D and 3D mathematical models of guided waves impinging on a hole and the resulting modal conversions were studied to understand the physical characteristics of the wave propagation in pipes. EMATs were developed for exciting the N_1 SH mode in pipes and were integrated into a PIG with data acquisition and data representation algorithms in place. Although flaw classification is possible using EMAT sensors, characterization of the flaws will require further study. Additional data and further wavelet analysis will be pursued to answer some of these questions.

References

1. Posakony, G.J., and Hill, V.L., "Assuring the integrity of natural gas transmission pipelines," Topical Report, GRI, Nov. 1992.
2. Khaleel, M.A., and Simonen, F.A., "Effects of alternative inspection strategies on piping reliability," Nuclear Engineering and Design, Vol. 197, pp. 115-140, 2000.
3. Thompson, R.B., "Physical Principles of Measurements with EMAT Transducers" Physical Acoustics, edited by W. P Mason, Academic Press, Vol. XIX, pp.157-199, 1990.
4. Gori, M., Giamboni, S., D'Alessio, E., Ghia, S., Cernuschi, F., and Piana, G.M., "Guided waves by EMAT transducers for rapid defect location on heat exchangers and boiler tubes," Ultrasonics, Vol. 34, pp. 311-314, 1996.
5. Gori, M., Giamboni, S., D'Alessio, E., Ghia, S., and Cernuschi, F., "EMAT transducers and thickness characterization on aged boiler tubes," Ultrasonics, Vol. 34, pp 311-314, 1996.
6. Hirao, M., Ogi, H., and Yasui, H., "Contactless measurement of bolt axial stress using a shear wave electromagnetic acoustic transducer," NDT&E international, Vol. 34, pp. 179-183, 2001.
7. Hirao, M., and Ogi, H., "An SH-wave EMAT technique for gas pipeline inspection," NDT&E International, Vol. 32, pp 127-132, 1999.
8. Gauthler, J., Mustafa, V., Chabbaz, A., and Hay, D.R., "EMAT generation of horizontally polarized guided shear waves for ultrasonic inspection," International pipeline conference, Vol. 1, ASME, 1998.
9. Hamilton, J.C., "The development of an EMAT based in-line inspection system for the detection of stress corrosion cracks in operating pipelines," GRI report 00/0184, April 2000.
10. Wilcox, P., Lowe, M., and Cawley, P., "The effect of dispersion on long range inspection using ultrasonic guided waves," NDT&E International, Vol. 34, pp 1-9, 2001.
11. Sawaragi, K., Salzburger, H.J., Hubschen, G., Enami, K., Kirihiyashi, A., and Tachibana, N., "Improvement of SH-wave EMAT phased array inspection by new eight segment probes," Nuclear Engineering and Design, Vol. 198, pp. 153-163, 2000.
12. Kwun, H., Hanley, J.J., and Holt, A.E., "Detection of corrosion in pipe using magnetostrictive sensor technique," Nondestructive evaluation of aging maritime, SPIE, Vol. 2459, pp. 140-148, 1995.
13. Kwun, H., and Hanley, J.J., "NDE of steel Gas pipelines using magnetostrictive sensors," GRI report, 95/0362, October 1995.
14. Guo, Z., Achenbach, J.D., and Krishnaswamy, S., "EMAT generation and laser detection of single lamb wave modes," Ultrasonics, Vol. 35, pp. 423-429, 1997.
15. Murayama, R., " Study of driving mechanism on electromagnetic acoustic transducer for lamb wave using magnetostrictive effect and application in drawability evaluation of thin steel sheets," Ultrasonics, Vol. 37, pp. 31-38, 1999.
16. Castaings, M., and Hosten, B., " Lamb and SH waves generated and detected by air coupled ultrasonic transducers in composite material plates," NDT&E International, Vol. 34, pp. 249-258, 2001.
17. Cho, Y., Rose, J. L., 1996. A Boundary Element Solution for a Mode Conversion Study on the Edge Reflection. *The Journal of the Acoustical Society of America* 99(4), 2097-2109.
18. Cho, Y., Rose, J. L., 2000. An Elastodynamic Hybrid Boundary Element Study for Elastic Guided Wave Interactions with a Surface Breaking Defect. *Int. J. Solids Structures* 37, 4103-4124.
19. Achenbach, J. D., 1998. Lamb Wave as Thickness Vibrations Superimposed on a Membrane Carrier Wave. *The Journal of the Acoustical Society of America* 103, 2283-2286.
20. Achenbach, J. D., Xu, Y., 1999. Wave Motion in an Isotropic Elastic Layer Generated by a Time-Harmonic Point Load of Arbitrary Direction. *The Journal of the Acoustical Society of America* 106, 83-90.
21. Chang, Z., Mal, A., 1999. Scattering of Lamb Waves from a Rivet Hole with Edge Cracks. *Mechanics of Materials* 31, 197-204.
22. Fromme, P., Sayir, M. B., 2002. Measurement of the Scattering of a Lamb Wave by a Through Hole in a Plate. *The Journal of the Acoustical Society of America* 111, 1165-1170.
23. Diligent, O., Grahn, T., Bostrom, A., Cawley, P., Lowe, M., 2002. The Low-Frequency Reflection and Scattering of the S0 Lamb Mode from a Circular Through-Thickness Hole in a Plate: Finite Element, Analytical and Experimental Studies. *The Journal of the Acoustical Society of America*.
24. Kerckel, S.W, Tucker, R.W., and Varma, V.K., "Pipeline flaw detection with wavelet packets and Gas", SPIE 2003.